Comparison of Monte Carlo methods for fluorescence molecular tomography—computational efficiency

Jin Chen and Xavier Intes[a)]
Department of Biomedical Engineering, Rensselaer Polytechnic Institute, Troy, New York 12180

(Received 29 May 2010; revised 3 August 2011; accepted for publication 30 August 2011; published 27 September 2011)

Purpose: The Monte Carlo method is an accurate model for time-resolved quantitative fluorescence tomography. However, this method suffers from low computational efficiency due to the large number of photons required for reliable statistics. This paper presents a comparison study on the computational efficiency of three Monte Carlo-based methods for time-domain fluorescence molecular tomography.
Methods: The methods investigated to generate time-gated Jacobians were the perturbation Monte Carlo (pMC) method, the adjoint Monte Carlo (aMC) method and the mid-way Monte Carlo (mMC) method. The effects of the different parameters that affect the computation time and statistics reliability were evaluated. Also, the methods were applied to a set of experimental data for tomographic application.
Results: *In silico* results establish that, the investigated parameters affect the computational time for the three methods differently (linearly, quadratically, or not significantly). Moreover, the noise level of the Jacobian varies when these parameters change. The experimental results in preclinical settings demonstrates the feasibility of using both aMC and pMC methods for time-resolved whole body studies in small animals within a few hours.
Conclusions: Among the three Monte Carlo methods, the mMC method is a computationally prohibitive technique that is not well suited for time-domain fluorescence tomography applications. The pMC method is advantageous over the aMC method when the early gates are employed and large number of detectors is present. Alternatively, the aMC method is the method of choice when a small number of source-detector pairs are used. © *2011 American Association of Physicists in Medicine*. [DOI: 10.1118/1.3641827]

Key words: Monte Carlo, time resolved, fluorescence tomography, small animal imaging

I. INTRODUCTION

Small animal imaging is emerging as a powerful tool in biological research and medical diagnosis to observe *in vivo* the biochemical, genetic, or pharmacological processes under study. Optical techniques utilizing fluorescent substances for small animal imaging have received steady attention in the last decade. The emitted photons from the fluorescently labeled targets can provide functional and molecular information by locating and tracking the bio-distribution of the targets in tissue, which is extremely valuable in drug development. Of particular importance is the combination of fluorescence imaging with tomographic techniques allowing three-dimensional visualization and quantification of biomarkers *in vivo*.

To perform quantitative fluorescence tomography, it is essential to employ an accurate mathematical model to describe the propagation of light in biologic tissues. The Monte Carlo method is a statistical method that tracks individual photons as they propagate. In the case of optical imaging, the interactions of the photon with the tissue are dependent on the scattering properties (scattering length and anisotropy), the absorption properties and in case of fluorescent the fluorophores properties (quantum yield, lifetime, quenching, etc.). This method is considered the gold standard to accurately model light propagation in either diffusing or nondiffusing media with flexibility to model arbitrary boundaries.[1] It is selected as the most accurate forward model to validate newly developed algorithms (based on the diffusion equation or the radiative transport equation) for fluence/flux prediction, and has been studied for years in spectroscopy and bulk optical properties reconstruction.[2–4] However, owing to the statistical nature of the Monte Carlo method, the propagation of a large number of photons must be simulated to attain reliable results. This makes the Monte Carlo method a computationally expensive technique for tomographic reconstruction. This computational burden, along with the memory constraints in early computers, has hindered the use of the Monte Carlo method as a forward model for tomographic reconstruction, since tomography requires simulating numerous source-detector (SD) pairs translating to orders of magnitude increase in calculation time. However, there is renewed interest in implementing the Monte Carlo method for tomographic use because of its appealing accuracy in modeling light transport for preclinical studies.[5–8] For instance, continuous wave weight functions based on the Monte Carlo simulations in an adjoint form have been applied to tomographic reconstructions in association with unmixing techniques fitting the decaying part of the time-domain data.[5,6] The perturbation Monte Carlo (pMC) method, utilizing the time-gated Jacobian of the forward Monte

Carlo simulations with respect to the spatial fluorophore distribution as the weight function, has also been successfully applied to fluorescence tomography in a computational efficient manner.[7]

It is noteworthy that the direct time-domain dataset (time gates) has unique benefits in fluorescence tomography due to the rich information content it carries which can improve quantitative accuracy, resolution[9,10] and perform lifetime multiplexing without the use of unmixing algorithms.[7,11] The Monte Carlo method is crucial when employing time-gated data not only due to its accuracy for a broad range of optical properties but also for modeling the early rising component (photon counts less than 50% of the maximum) of the temporal point spread function (TPSF), where the approximation to the transport equation, namely the diffusion equation, fails.[1] However, photons are split into small time-bins (gates) in time-domain Monte Carlo implementations, leading to a significant increase in computation time to achieve reliable statistics for each individual gate. With the recent progress in parallel computing, tomography employing time-gated Monte Carlo method is becoming viable thanks to the acceleration based on massively parallel computation.[7] Besides the pMC method, the forward-adjoint Monte Carlo (aMC) method, and the mid-way Monte Carlo (mMC) method have been previously used to optimize the efficiency of the forward Monte Carlo calculations, however, to our knowledge, implementation in time-gated tomography has not yet been reported. In this work, we have extended the aMC and mMC methods to time domain for the calculation of direct Jacobians and benchmark them with our previously developed the pMC method, in terms of the time efficiency for full tomographic reconstruction settings. We report herein the computational comparison of these three Monte Carlo methods in generating time-gated Jacobians for full tomographic reconstructions on the same computational platform for time resolved FMT applications.

II. METHOD

The distribution of the fluorophore can be reconstructed by solving an inverse problem that relates the detected signals collected at the surface of the sample to the local fluorophore-related parameters. In FMT applications, the Jacobian of the forward operator with respect to these parameters is commonly used to form a discrete linear inverse system. The fundamental difference of our three investigated Monte-Carlo-based techniques resides in the methods to form the Jacobian, which are conceptually depicted in Fig. 1.

The aMC method [cf. Fig. 1(a)] calculates the Jacobian by multiplying the resulting light fields from a forward simulation with photons propagating from the source position r_s and another one with an assumed source at the detector position r_d (adjoint simulation).[12] In the pMC method [cf. Fig. 1(b)], the Jacobians for multiple detectors can be directly generated from the stored photon path information in a single forward simulation for the source r_s. The mMC method [cf. Fig. 1(c)] employs a half-space forward simulation and a half-space adjoint simulation for one SD pair. These simulations treat all

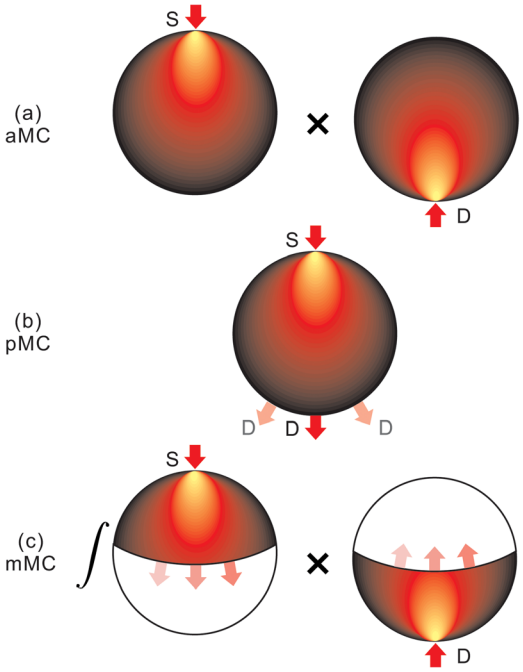

FIG. 1. The schematic diagram of the three Monte Carlo-based methods to create the sensitivity map of photon propagation with respect of the fluorescence change.

subsurfaces on the mid-surface as detectors, and calculate Jacobians and photon responses for all of them. For a certain subsurface, the half-space Jacobian calculated in the forward simulations is multiplied by the response generated from the adjoint simulation, and vice versa. Then, an integration of all these Jacobians over the mid-surface results in the final Jacobian for this SD pair. The three methods are described in detail in Secs. IIA-IIC.

II.A. Forward-adjoint Monte Carlo method

The aMC method has been proven efficient when the sources and detectors are small relative to the target volume, such as the point sources and detectors widely used in tomography.[5] However, because the Jacobian is the product of the source field and the detection field, this method can suffer from high variance on the boundaries.[13] The forward-adjoint Monte Carlo method is readily expanded to the time-domain method by introducing a time variable t.[14] According to the transport theory, the fluorescence intensity measured at r_d and time t for an impulsive excitation at r_s and $t_0 = 0$ can be written as:

$$U_F(r_s, r_d, t) = \int_\Omega dr \int_0^t dt' \int_0^{t'} dt'' \, G^x(r_s, r, t' - t'') \times G^m(r, r_d, t'')\eta(r)e^{-(t-t')/\tau}. \quad (1)$$

where the integration domain Ω is defined as the entire imaging volume and $\eta(r)$ is the yield distribution. The Green's functions G^x and G^m are the time-dependent background Green's functions for light propagation at the excitation and emission wavelengths, which can be solved analytically or numerically. Equation (1) can be written in a more concise linear form:

$$U_F(r_s, r_d, t) = \int_\Omega dr\, W(r_s, r_d, r, t)\eta(r), \tag{2}$$

where $W(r_s, r_d, r, t)$ is the weight function of the measurement $U_F(r_s, r_d, t)$ with respect of $\eta(r)$:

$$W(r_s, r_d, r, t) = \int_0^t dt'\, e^{-(t-t')/\tau} \int_0^{t'} dt'' \times G^x(r_s, r, t' - t'')G^m(r, r_d, t''). \tag{3}$$

Note in Eq. (3) a double convolution in time is required to calculate the full weight function, which affects the time efficiency of this method. In this study, the Monte Carlo method is employed to calculate the Green's functions $G^{(x,m)}$ instead of the ubiquitous diffusion equation at the excitation and emission wavelength. To calculate $G^x(r_s, r, t)$, a forward Monte Carlo simulation with particles starting at a source and traveling toward the detector is applied. Conversely, the adjoint Monte Carlo simulation calculates $G_n^m(r, r_d, t)$ following backward propagating photons from the detector to the target volume based on the general reciprocity theorem and originates when the transport from r to the r_d is replaced by adjoint transport from r_d to r.[15]

II.B. Perturbation Monte Carlo method

The time-gated pMC method for fluorescence tomography has been recently presented by directly utilizing the photon path information in the forward Monte Carlo method for fluorescence generation.[7] The double convolution in Eq. (3) can be written as two separate equations:

$$W(r_s, r_d, r, t') = \int_0^t dt'\, W'(r_s, r_d, r, t)e^{-(t-t')/\tau} \tag{4}$$

and

$$W'(r_s, r_d, r, t') = \int_0^{t'} dt''\, G_n^x(r_s, r, t' - t'')G_n^m(r, r_d, t'') \tag{5}$$

In the pMC method, assuming the same optical properties at the excitation and emission wavelength, the background weight function W' can be calculated implicitly based on

$$W'(r_s, r_d, r, t') = \sum_{i=1}^{n} w_i^x(r_s, r_d, t')\mu_a^x(r)l_i(r), \tag{6}$$

where n is the total number of photons propagating from r_s, passing through r and detected by the detector r_d at time t, w_i is the detected weight of the ith ($i = 1,\ldots,n$) photon, and $l_i(r)$ is the path length that the photon passes at r. Thus, the weight function is the weighted average of the photon paths at each sub-region and time-bin. If the absorption coefficients are different between the excitation and emission wavelengths, Eq. (6) can be modified to accommodate the difference by adding a correction term:

$$W'(r_s, r_d, r, t') = \sum_{i=1}^{n} w_i^x(r_s, r_d, t')\mu_a^x(r)l_i(r) \times \exp\left(-\sum_{j=p_i+1}^{q_i} \Delta\mu_a(r_j)\right), \tag{7}$$

where $\Delta\mu_a = \Delta\mu_a^m - \Delta\mu_a^x$ is the difference between the absorption coefficients at emission and excitation wavelengths, $r_j (j = 1,\ldots,q_i)$ are the regions that the ith photon passes from r_s to r_d and the p_ith region is r. Since the Monte Carlo simulation stores the path histories for each sub-region within the volume of interest, any distribution of absorption coefficient at the excitation and emission wavelengths can be rapidly simulated. Moreover, this formulation allows to compute fluorescence Jacobians for all the detectors and time simultaneously in a computationally efficient manner by allocating the memory to store the time-resolved weight matrix for each detector.

II.C. Mid-way Monte Carlo method

In either the forward or the adjoint run in the mMC method, the photons propagate up to a customized midway surface that spatially separates the source and the detector. The detector response can then be estimated by an integral of the product of the radiation current of the forward and the adjoint functions on the midway surface. Up till now, the method has been developed for time-dependent forward problems and validated for several test cases.[16,17] It has been shown to be particularly efficient in problems that involve deep penetration and/or complex paths taken by the radiation as it moves from source(s) to detector(s), which can be also encountered in the optical tomography. Assuming isotropic pairing at the surface, the method can be expressed as

$$U_F(r_s, r_d, t) = \int_0^t dt' \int_0^{t'} dt'' \int_S dr_S\, \psi(r_s, r_S, t' - t'') \times \psi(r_d, r_S, t'')e^{-(t-t')/\tau}, \tag{8}$$

where S denotes the midway surface, $\psi(r_s/r_d,r_S,t)$ is the response at t, and at a subsurface r_S on S due to a source located at r_s/r_d. Note that the midway surface totally encompasses the source/detector but excludes the detector/source, hence, the calculation for ψ only occurs in part of the volume. In order to generate the Jacobian using this method, we expand ψ as a linear function of η over the partial volume Ω_s/Ω_d including r_s/r_d:

$$\psi(r_s/r_d, r_S, t) = \int_{\Omega_s/\Omega_d} dr\, W'(r_s/r_d, r_S, r, t)\eta(r), \tag{9}$$

where W' can be calculated by Eqs. (4),(6), or (7). Since using the adjoint method [Eq. (5)] requires simulating every subsurface at S as a source, we used the pMC method to calculate the Jacobian for all the subsurfaces simultaneously. That is, to save the paths for every subsurface on the midway surface, then pair the photons that reach the subsurface in the forward run and the adjoint run. In this implementation, we stored the paths on the computer hard disk to create the matrix for every subsurface.

II.D. Computational settings

The BlueGene cluster at the Computational Center for Nanotechnology Innovations (CCNI) at Rensselear Polytechnic Institute was employed for all computations herein. This

cluster consists of 16,384 nodes with two single-thread 700-MHz PowerPC 440 CPUs and 512 or 1024 MB of DDR DRAM per node. The interconnect network structure is a three-dimensional torus with a transfer speed of 175 MBps in each direction and global collective rate of 350 MBps with 1.5 μs latency.

The forward Monte Carlo simulations in this work were based on the conventional forward Monte Carlo routine for light propagation.[18] That is, the photons are propagating from an initial position then scattered based on the Henyey–Greenstein phase function, while the photon weights are decreasing along the travel paths. The method was implemented in C and incorporated with the communication protocol MPI for parallel computing on clusters/supercomputers and compiled on a 32-bit UNIX-like proprietary operating system for BlueGene. In the pMC and mMC approaches, several nodes were allocated to store the photon paths and the number of these nodes was adapted to the size of the problem and memory of the node. Since the Monte Carlo approach is highly parallizable, the increase in time efficiency is approximately linear to the increase of the calculating nodes. In this particular work, the number of total nodes used for Monte Carlo calculations was fixed to 4096, which is the maximum for job requests on BlueGene.

Besides the hardware/software settings, there are various parameters affecting the time cost of Monte Carlo simulations to generate the Jacobians. In this study, simulations with different numbers of photons, numbers of sources/detectors, numbers of gates, gate widths, voxel sizes, and optical properties, were evaluated to compare the time efficiency. The objective of this investigation was to reveal the relationship of the time cost changes with respect to any change of these parameters for the different methods of Jacobian calculation. The range for each parameter was selected, according to general preclinical system settings and listed in Table I. These parameters are independent to each other, thus the evaluations were conducted by changing one or two parameters at a time while keeping the other parameters constant. The fixed values are also listed in Table I. It is noteworthy that for the optical properties, only the scattering coefficient μ_s was considered as a parameter affecting the time efficiency, because any changes in μ_a can be easily scaled by using the stored photon paths when the scattering is fixed.[19] In investigating the effect of μ_s, simulations with a series of μ_s' were evaluated with $\mu_a = 0.3$ cm^{-1}, $g = 0.9$, and $n = 1.37$, which are all typical values for mouse tissue in the Near-infrared (NIR) spectral region.[20] A $4 \times 4 \times 2$ cm slab was employed in all the simulations (cf. Fig. 2), where the thickness of the model was mimicking the maximum thickness of a murine model.

TABLE I. Parameter range for time efficiency evaluation.

Parameter	Notation	Range	Fixed value
Number of photons	N_{photon}	10^5–10^9	10^9
Number of sources	N_s	1–256	1
Number of detectors	N_d	1–1024	1
Number of gates	N_{gate}	1–60	60
Gate interval	T_{shift}	20—60 ps	40 ps
Gate width	T_{gate}	200—800 ps	200 ps
Voxel size	V_{voxel}	0.5^3–2^3 mm^3	1 mm^3
Scattering coefficient	μ_s'	5—25 cm^{-1}	15 cm^{-1}

II.E. Statistical criteria for computational efficiency comparison

Like the forward Monte Carlo simulations, the accuracy in Monte Carlo-based reconstruction approaches is fully dependent on the spatial and temporal statistical characteristics of the Jacobian. However, the statistical characteristics of the Jacobians calculated by the methods investigated herein may be different utilizing the same number of photons. Moreover, changes in scattering may also lead to a change in statistics, due to altered photon paths distribution. Therefore, analyzing only the time cost with the same number of photons is not sufficient. Lastly, different selections of gate widths and voxel sizes may cause variation in statistics. Hence, it is critical to determine the least number of photons for each approach to generate Jacobians reaching the required fidelity for stable and accurate reconstructions.

Hence, we compared the generated Jacobians for the central SD pair at the middle plane (cf. Fig. 2) to a precomputed reference Jacobian. We employed an objective error metric where the error ϵ at position r was defined as

$$\epsilon(r) = \left| \frac{v(r) - v_{\text{ref}}(r)}{v_{\text{ref}}(r)} \right| \times 100\%. \tag{10}$$

In Eq. (10), $v(r)$ and $v_{\text{ref}}(r)$ were the values at r of the generated and reference Jacobians, respectively. The average of ϵ for the middle plane voxels was denoted as $\bar{\epsilon}$. The Jacobian using the pMC method with 10^{10} photons was chosen as the reference, as the difference between two independent calculations with 10^{10} photons leads to an error ($\bar{\epsilon}$) less than 1% in CW. Additionally, based on a previous study, the pMC method using 10^9 photons can provide a stable and accurate reconstruction in time-gated FMT (Ref. 7) with an average error around $\bar{\epsilon} = 5\%$ in the Jacobian. Thus, when $\bar{\epsilon}$ reduces to 5%, we consider the Jacobian to be statistically stable for reconstructions.

First, we investigated the performance of the three methods in continuous wave mode (CW) with different μ_s' to obtain an initial estimate of the required N_{photon}. The CW

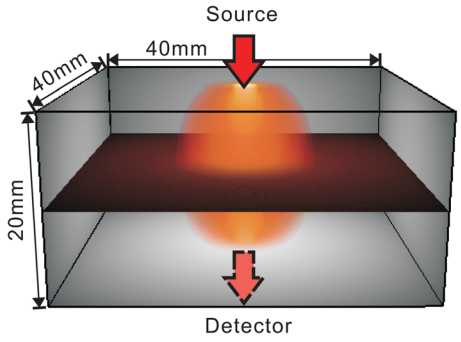

FIG. 2. The slab geometry used in the middle plane statistics comparison. An example Jacobian for the assigned SD pair is shown too.

Jacobian was generated by integrating the excitation photons arriving at the detectors over a 2 ns span (in simulations after 2 ns the detected excitation photons is typically less than 0.5% of the total). Second, in order to determine N_{photon} for statistically stable time-domain reconstruction, we tested our approaches on the same geometric settings. We employed 200 ps gates with 20 ps interval between gates, which is the highest temporal resolution our imaging platform can achieve for a full time window of 4 ns for fluorescence signal detection. The number of the photons in time-domain simulations was increased by 10 over the CW case based on the ratio of the CW time span and the gate width. The effect of different T_{gate} and V_{voxel} on statistics was then investigated for the time-domain data.

II.F. Reconstructions based on experimental data

To demonstrate the effect of different statistical characteristics of the Jacobians on reconstructions under a practical scenario, the performances of the methods were also evaluated experimentally for time-resolved whole body FMT. The data were acquired from an *in vivo* experiment using a newly developed time-resolved wide-field tomography platform at RPI [cf. Fig. 3(a)].[21] The system employed a tunable femtosecond laser as the source and a time-gated ICCD camera as the detector. A pico-projector module was used for source pattern generation allowing rapid acquisition of spatially and temporally dense measurements. The experiment was performed on an euthanized mouse implanted with a fluorescent capillary filled with Indocyanine green (ICG) [cf. Fig. 3(b)].[10] We limited the volume to be imaged to the chest section (36×24 mm). 64 half-space patterns sliding along with x- and y-axis were employed as illumination source, with 97 detectors having a separation of 1.5 mm under a transmittance geometry on the platform. We acquired a profile covering 4.6 ns with 40 ps shift between the gates, resulting in 115 gates recorded. The gate width were set to 300 ps to achieve an adequate signal-to-noise ratio and also retain high sensitivity to the short lifetime.[21]

The outer shape of the mouse was extracted as the boundary for photon transport in the Monte Carlo simulations. The optical properties for the whole mouse were set to the average background properties of small animals ($\mu_a = 0.3$ cm^{-1}, $\mu_s' = 15$ cm^{-1}). Combining these surface measurements, a linear system was formed based on the born normalization form of Eq. (2) to minimize the effect of the heterogeneous background. The conjugate gradient method was applied to solve this linear system, with a fixed iteration number of 50. Note that all the simulations and reconstructions were employed without any internal structural information as *a priori* constraint.

III. RESULTS AND DISCUSSION

In Sec. III A, the required N_{photon} for each method in CW is estimated. The effects of the efficiency-related parameters for time-gated calculations are then evaluated in Sec. III B and the N_{photon} for stable time-gated reconstruction is determined in Sec. III C. The time cost for generating Jacobians for multiple SD pairs for tomography is evaluated subsequently in Sec. III D. Lastly, whole-body tomographic reconstructions in a small animal model using the aMC and pMC methods are provided in Sec. III E for comparison for the three methods.

III.A. Computational efficiency in CW

We first investigate the effect of the change in N_{photon} and μ_s' on the Jacobian statistics for the central SD pair. Figure 4 presents the result of increasing N_{photon} vs mean error at the middle plan ($\bar{\epsilon}$) for different background μ_s' in CW. For all methods, an increase of N_{photon} results in a reduction of the average error $\bar{\epsilon}$, implying an improvement in statistics. The rate of change in $\bar{\epsilon}$ is decreasing with respect to the increase of N_{photon}. That is, when N_{photon} is relatively small (10^5–10^6), an increase in N_{photon} results in a marked decrease of error. However, when $\bar{\epsilon}$ reaches a certain level (e.g., 5%), an increase in N_{photon} does not reduce $\bar{\epsilon}$ significantly. Thus, the threshold of N_{photon} (for $\bar{\epsilon} < 5\%$) is important to avoid the calculation burden, as simulating more photons does not lead to a significant improvement in Jacobian statistics, and hence reconstruction quality.

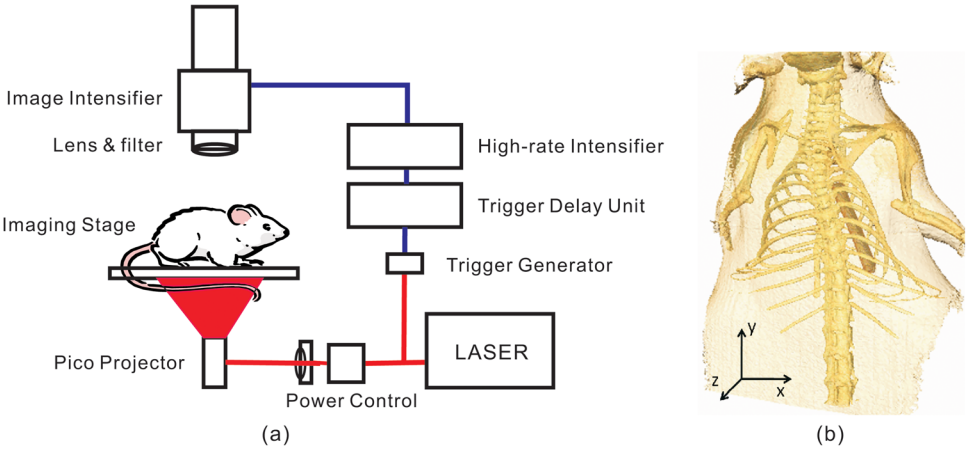

FIG. 3. (a) The experimental platform for the whole body time-resolved FMT in small animals. (b) Anatomical data of the mouse acquired by Micro CT.

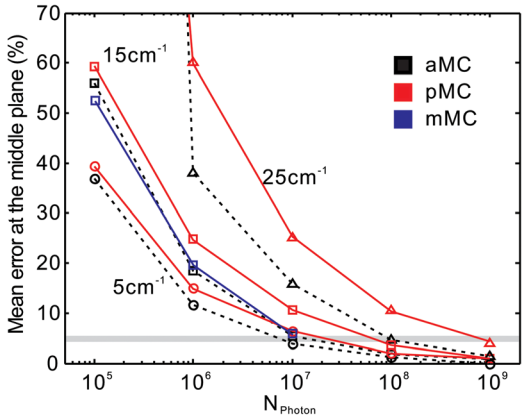

FIG. 4. The mean error at the middle plane of the Jacobian ($\bar{\epsilon}$) along with the increase of photons for different Monte Carlo approaches in CW.

For the average murine $\mu_s' = (15\ \mathrm{cm}^{-1})$, the aMC method requires ~20% ($10^7 \times 2$) of N_{photon} compared to the pMC method (~10^8) to reach the same level of statistics ($\bar{\epsilon} < 5\%$). This difference of required N_{photon} for aMC and pMC methods stands from the fact that, for one source and detector, only the photons received by the detector are recorded in the pMC method, but all the simulated photons (in the forward run and adjoint run) are recorded in the aMC method and contribute to the statistics. However, the statistics of the Jacobian generated by the pMC method can be improved by increasing the size of the detector to receive more photons, which is appealing for the recent implementation of wide-field detection.[22] The statistics changes at the middle plane using the mMC and aMC methods are close to each other (<5% difference), due to the similarity of the two methods, that is, the forward and adjoint simulations and the convolution in time are involved in calculation for both methods. We only show up to 10^7 photons for the mMC method due to the lengthy calculation time to generate the Jacobian using this method (Table II).

The change of background μ_s' has an important influence on the statistical characteristics of Jacobian. As expected, an increase in μ_s' results in an increase of error, that is, with higher μ_s', significantly more photons are required in the Monte Carlo simulations to achieve reliable statistics. This can be explained by the fact that the higher μ_s' the more uniformly the photons distribute in the examined region, leading to a less photon count in a certain sub-region thus a decrease in statistics. This result suggests that the optimal number of photons used for generating the Jacobian should vary according to μ_s' to assure an satisfying reconstruction.

The time cost for CW simulations for average murine optical properties producing results with less than 5% error at the middle plane are listed in Table II. The computation time for the aMC method to calculate the Green's function using 10^7 photons is about 4–5 s for a single source or detector (10 s for one SD pair). For tomography applications, the number of simulations is linear to both N_s and N_d based on the forward adjoint formulation as all simulations for sources and detectors are independent and additive. The time cost for the pMC method using 10^8 photons is ~1 min for one SD pair. However, the time cost for the pMC method remains almost constant (under 6% change) when the number of detectors increases. This is because, the photon paths are transferred to different nodes corresponding to different detectors therefore reducing the waiting time for data transfer at the calculation nodes. This transfer process results in an increase of 5%–15% to the time cost for an aMC simulation at the same source with the same number of photons. In summary, the aMC method is more efficient for a small number of N_s and N_d, and the pMC method is more efficient when a large N_d is employed.

Conversely, the mMC implementation to generate the Jacobian for tomography use is practically difficult. In this study, voxel-size subsurfaces are used at the middle plane and the number of the subsurfaces (40×40) is greater than N_d used in tomography (<500). Therefore, the main constraint is the hardware memory capacity that limits the size of the volume that can be reconstructed. On the other hand, if the photon paths are stored on the disk, as in this implementation, it leads to lengthy writing and reading times. From Table II, the time cost using the mMC method with 10^7 photons is more than 10 h for a small number of SD pairs (36×36), due to the time-consuming process to read and pair the photon paths at the mid-plane. This process is even more unpractical in the time-domain for which the pairing of the photons should be done per time-gate. Therefore in the rest of this paper, we disregard the mMC method.

TABLE II. Total time cost for same level of statistics (CW).

N_s	N_d	aMC (10^7)	pMC (10^8)	mMC (10^7)
1	1	~9 s	<1 min	<10 min
1	64	~5 min	<1 min	~5 h
1	256	~18 min	~1 min	~25 h
36	36	~5 min	~30 min	~10 h
36	64	~7 min	~30 min	~15 h
36	256	~21 min	~30 min	~40 h
36	1024	~75 min	~32 min	—

III.B. Time-domain computational efficiency

The observed effects of the parameters listed in Table I on the computational time are summarized in Table III for time-domain simulations. The big- O notation is used for analyzing the correlation between the examined parameter n and the calculation time. It represents the order of the dominant term for n when n tends toward the maximum value listed in Table I. Overall, the effect of these parameters on the total time cost is $O(n^2)$ (quadratic), $O(n)$ (linear), or $O(1)$ (constant). For instance, N_{photon} is linearly related to the

TABLE III. The effects of different parameters on total time cost.

	N_{photon}	N_s	N_d	N_{gate}	T_{shift}	T_{gate}	μ_s'	V_{voxel}
aMC	$O(n)$	$O(n)$	$O(n)$	$O(n^2)$	$O(1)$	$O(1)$	$O(n)$	$O(n)$
pMC	$O(n)$	$O(n)$	$O(1)$	$O(1)$	$O(1)$	$O(1)$	$O(n)$	$O(n)$

calculation time due to the additive nature of simulating more photons. As expected, the relationships of simulation time cost with N_s and N_d remain the same as in CW as these parameters are not related to time. The effect of N_d for the aMC and pMC simulations can also be observed in Figs. 5(a) [$O(n)$] and 5(b) [$O(1)$]. However, the total time cost for generating the Jacobian using the aMC method includes not only the simulation time [cf. Fig. 5(a)] but also the convolution time [cf. Fig. 5(c)]. The convolution time increases linearly with the increase of N_d, which is the same as for the simulation time. Thus, the effect of N_d on the total time is linear [$O(n)$]. The effect of N_{gate} on the time cost is however different for the simulation time and convolution time. The time for simulations using the aMC method tends toward constant [$O(1)$] along with increasing N_{gate} because most of the photons have propagated outside of the tissue after a certain time point (for 20 ps T_{shift}, gates later than gate 50 receive $<2\%$ of the total photons). The convolution time when using the aMC method has a quadratic dependence [$O(n^2)$] on N_{gate}. Moreover, it becomes more dominant when the number of SD pairs increases. The time cost for the pMC method [cf. Fig. 5(b)] only consists of the forward simulation time thus increases toward constant [$O(1)$] along with increasing N_{gate}, similarly. For increasing T_{shift} and T_{gate}, the calculation time also tend to a constant (the CW calculation time) once the combination of T_{shift}, T_{gate}, and N_{gate} covers all photons time of flight. The change in μ_s' is linearly related to the change of the average number of scattering in Monte Carlo simulations so as to the calculation time [cf. Fig. 5(d)]. An increase of scattering coefficient from 5 to 25 cm^{-1} results in an increase of the calculation time by $\sim$60%. For the average scattering coefficient 15 cm^{-1}, the calculation time is around 8 min (480 s) for the pMC method (10^9) and $\sim$48 s for the aMC method (10^8, one forward or adjoint simulation). By increasing V_{voxel}, the calculation time linearly decreases due to the increased density of grid. However, this change is not significant ($\leq$8%) because the photon paths are not changed statistically.

III.C. Statistics of time-domain Jacobians

The result of statistics comparison for time-gated Jacobian calculations for the aMC and pMC methods using 10 times the required number of photons to obtain stable CW Jacobians (10^7 and 10^8) is shown in Fig. 6 (10^8 and 10^9). The Jacobians calculated by the aMC method have a marked

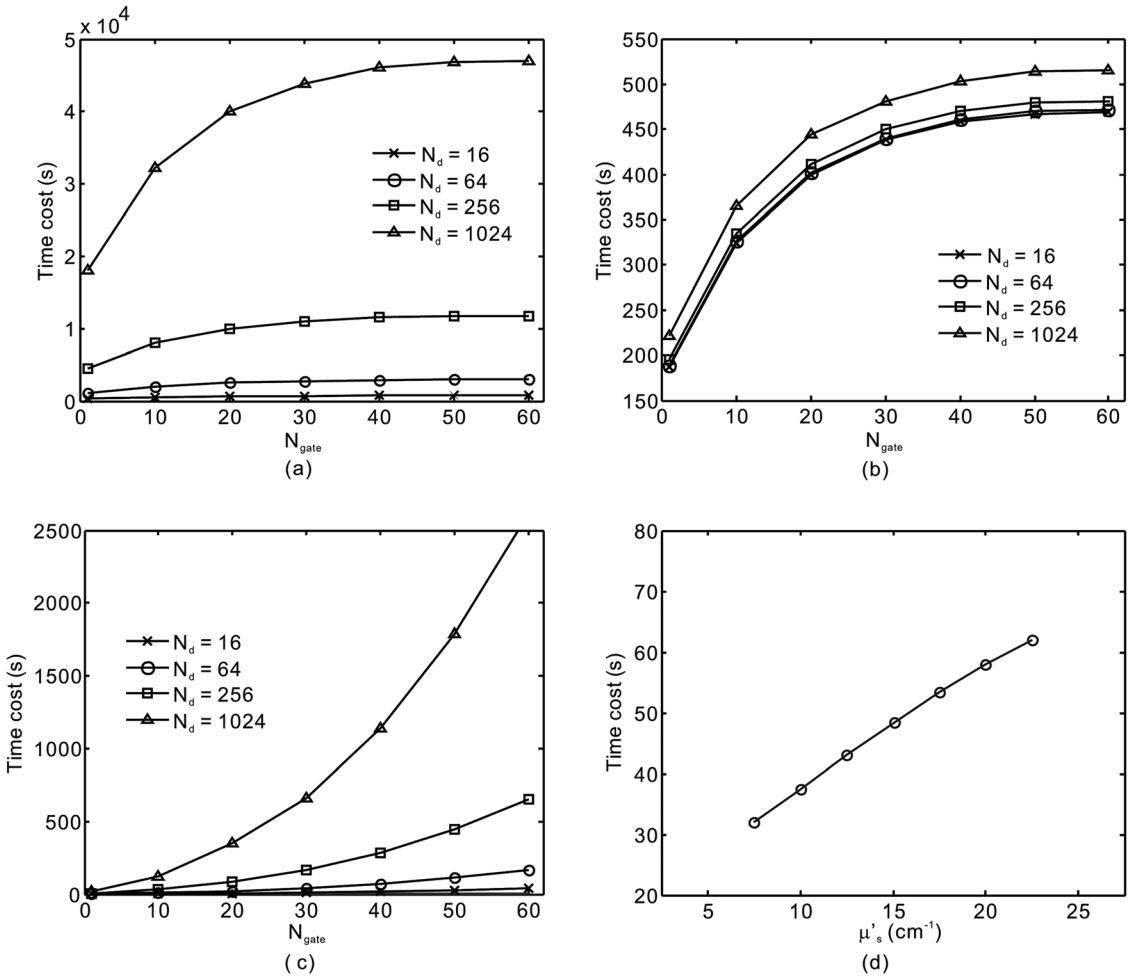

FIG. 5. The computational time for simulations with $N_s = 1$ and $N_d = 16$, 64, 256, and 1024 using the (a) aMC and (b) pMC methods. (c) The calculation time for the convolution in the aMC method. (d) Time cost using different μ_s' for the aMC method with 10^8 photons.

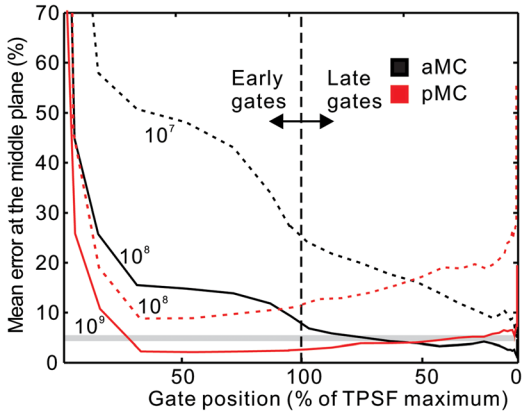

FIG. 6. The mean error at the middle plane of the Jacobian ($\bar{\epsilon}$) at different time-gates for the aMC and pMC methods.

decrease in error along with the gate position moving toward the late gates, for which the Jacobian is calculated by convolving more gates based on Eq. (1). The double convolution in time summing up the photons detected in a full time span gives an equivalent result in $\bar{\epsilon}$ as in CW, thus $\bar{\epsilon}$ for both aMC calculations reaches a value close to that in CW using the corresponding number of photons. By increasing N_{photon}, the statistics becomes better as expected. The $\bar{\epsilon}$ for the pMC calculations reaches the minimum at around the 25% rising gate. This result does not exactly follow the rule that the statistics are only dependent on the number of photons that the detector receives. This is because, based on the defined statistics criteria, the sum of the percentage error is averaged to the whole middle plane. The statistics of $\epsilon(r)$, which is dependent on the number of photons at r, thus becomes worse around the boundary of the Jacobian. However, the shape of the Jacobian is expanding as time increases due to the increased probing area of photons detected by later gates [cf. Fig. (7)]. With more photons probing the boundary, more voxels with worse statistics are encountered at the late gates, resulting in an increase of $\bar{\epsilon}$. The statistics of Jacobian calculated by the pMC method with 10^9 photons is stable (almost all around the 5% line) after the ~25% rising gate compared to that with 10^8 photons. The change of $\bar{\epsilon}$ in this range is within 4%, which makes it more suitable for reconstructions using gates at any position of the whole time span. $\bar{\epsilon}$ reaches 5% for the aMC method with 10^8 photons after the maximum gate, whereas for the pMC method with 10^9 photons at around 25% rising gate. The Jacobians for early and late gates are shown in Fig. 7. At the early gate, Jacobian by the pMC method (10^9) shows closer statistics to the reference [cf. Figs. 7(d) and 7(e)] compared to that by the aMC method(10^8), whereas at the late gates, these two methods have equivalent performances.

By increasing T_{gate} or V_{voxel}, the statistics are improved because more photons are accumulating in a wider gate or a larger volume, as shown in Figs. 8(a) and 8(b), respectively. However, the increase of photons does not affect the statistics in the same way for the two Monte Carlo-based methods. For the aMC method, due to the convolution in time, the Jacobian for a specific gate includes the information for any gate earlier than it. Increasing the gate width results in the photon path information recorded over a later time bin to be added to the original gate. As a result, the decrease of error for the early gate by increasing T_{gate} is greater than that for the late gates, because for early gates, the photons detected in the added time bin (toward maximum gate) are more than that for late gates (toward later gate receiving less photons). For the pMC method, the Jacobian for a gate only contains the information of the photons detected in this gate but not any gate ahead of it. For the early gate, increasing T_{gate} from 200 to 400 ps will add the information for the photons around the maximum gate (~320 ps) and the improvement is significant with an error close to that for the maximum gate. The improvement is small by increasing T_{gate} afterward because the received photons are minimum after $t = 500$ ps. This also explains that for late gates, increase in T_{gate} does not change the error. The difference of the Jacobians using 1 and 8 mm^3 on statistics is fairly small (within 6%), whereas by increasing the voxel size from 0.125^3 to 1 mm^3 the rate of change in error is significant. This result implies that for this simulation setting, using 1 mm^3 voxels is equivalent to using 8 mm^3 voxels in statistics, without decreasing the resolution in reconstructions.

III.D. Generating multiple Jacobians for tomography

In tomographic settings, dense source-detector pairs are usually employed. Here, we examine the time efficiency of the aMC and pMC methods in a manner that $N_d = N_s$ and $N_d = N_s \times 4$ to mimic measurements acquired by CCD cameras. Figure 9 shows the time costs to generate a full set of Jacobians for reconstruction for all the gates (the aMC

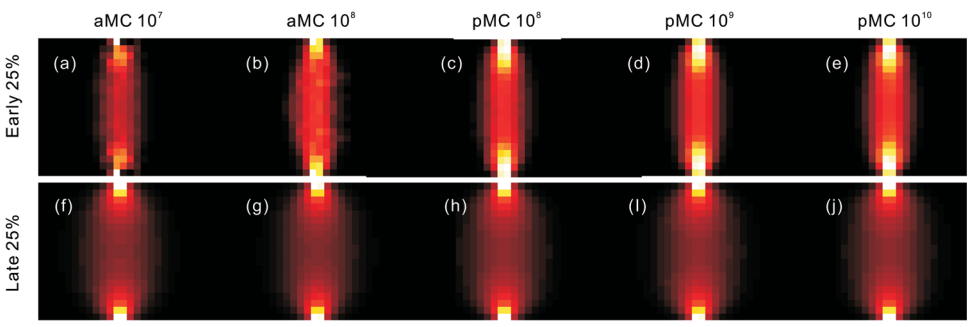

FIG. 7. A slice of the normalized Jacobians at the 25% rising and decaying gates, calculated by the aMC and pMC methods with different N_{photon}.

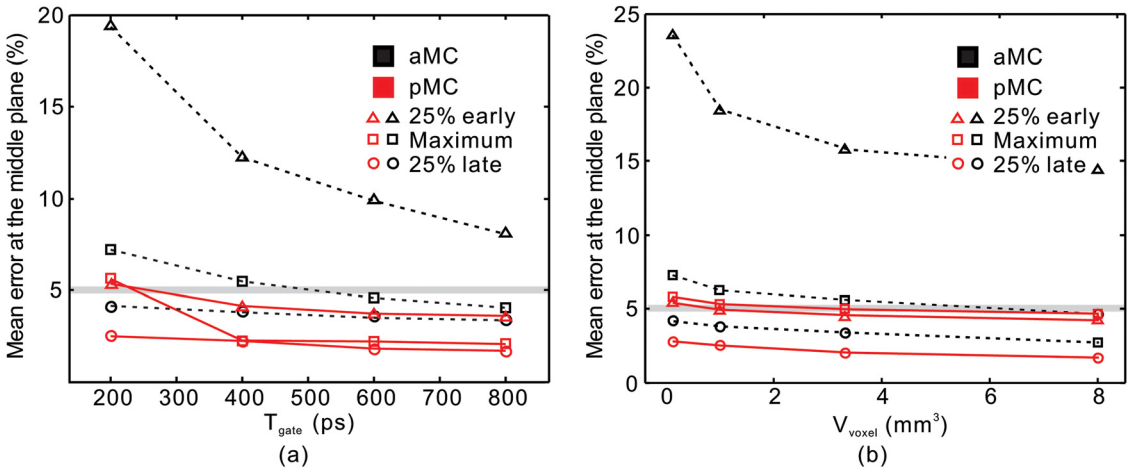

FIG. 8. The mean error at the middle plane of the Jacobian ($\bar{\epsilon}$) using different (a) T_{gate} and (b) V_{voxel}.

method with 10^8 photons and the pMC method with 10^9 photons). Note that the convolution time for the adjoint method becomes dominant when the number of SD pairs increases, which implies that, even if the forward Monte Carlo simulations are accelerated by using parallel computing, the required convolution still takes long if the number of SD pairs is large. The total time for the pMC method is less than that for the aMC method when $N_s = N_d > 150$. When N_d is much greater than N_s, the two methods shows nearly identical time efficiency when $N_s < 50$, but the pMC method shows superior efficiency otherwise. However, this is the case when the Jacobian for all the gates is generated. If certain gates are selected for reconstruction, e.g., early gate for resolution, the convolution time will decrease dramatically. For a single gate, the convolution time will be 2%–6% of the total convolution time, according to the position of the gate. This fact makes the aMC method an appealing approach if only a few gates are optimally selected for reconstruction. Practically, 5–10 gates are usually selected for reconstruction. In this case, the time cost for convolution can be reduced up to 90% leading to computational times almost equivalent to that for only forward simulations (dotted lines in Fig. 9), where the aMC method is more efficient than the pMC method for these SD combinations. Moreover, the computation for the convolution in the aMC method is performed under MATLAB and can be optimized for greater computational efficiency. The convolution time is expected to be reduced significantly by optimized computational methods, such as parallel acceleration using multicore CPU or graphics processing unit (GPU).[23] In summary, for tomographic systems with high spatial and temporal resolution, the pMC method can be more efficient than the aMC method, while for simpler fiber-based systems with the capability of acquiring less resolved signals, the aMC method is more suitable.

III.E. Experimental comparison

The single gate (25% rising) reconstruction result for the experimental data using the pMC and aMC method are shown in Fig. 10. Both aMC (with 10^8 photons) and pMC (with 10^9 photons) methods provide accurate reconstructions in terms of the position and shape of the object. Although there is a difference in the statistics for the two methods at

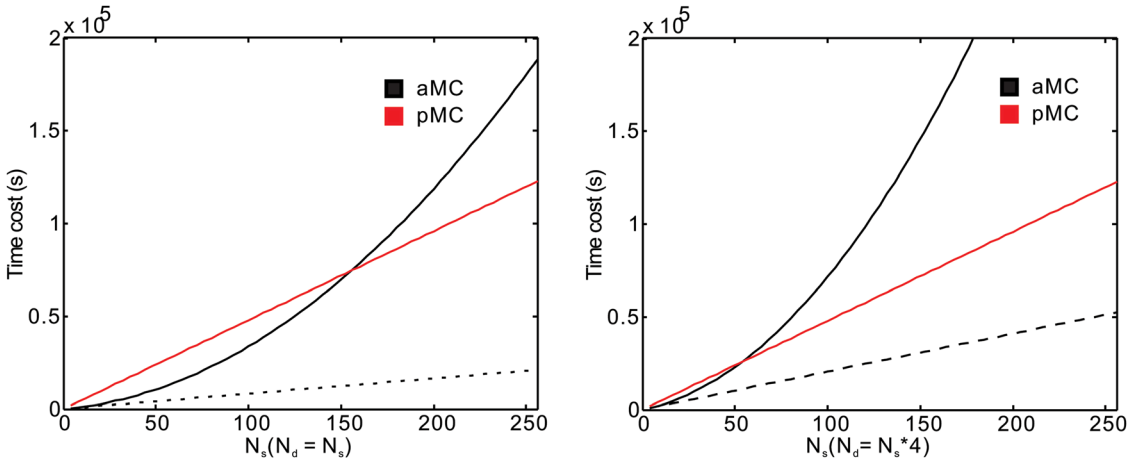

FIG. 9. The time cost to generate a full time-domain Jacobian when (a) $N_d = N_s$ and (b) $N_d = N_s \times 4$. The dashed lines in both figure represent the calculation time for the forward simulations using the aMC method.

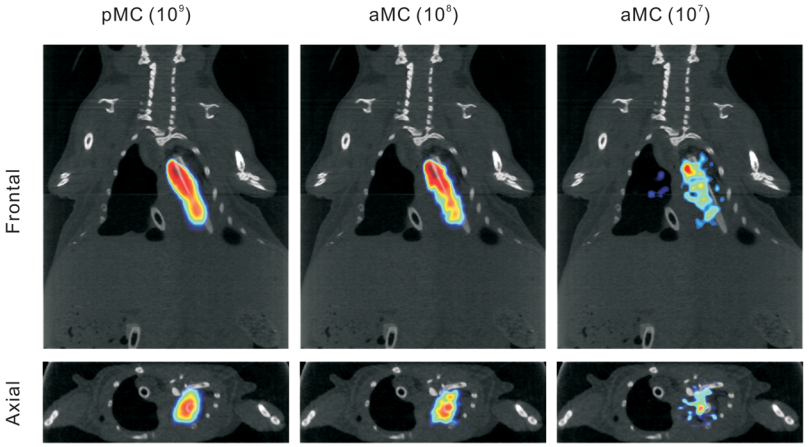

FIG. 10. The 25% rising gate reconstruction using (a) the pMC method with 10^9 photons, (b) the aMC method with 10^8 photons, and (c) the aMC method with 10^7 photons. The optical reconstructions are performed without any anatomical priors besides the external body boundaries. The optical reconstructions are overlaid on the Micro CT image for visualization/validation only.

this gate, the average for the voxels within the isovolume at half of the maximum reconstructed value is within 6%. For comparison, the result using the aMC method with 10^7 photons is also shown in Fig. 10. With this number of photons, incorrectly reconstructed artifacts due to the noise can be observed, demonstrating that reliable statistics is essential in reconstructions.

The experimental platform with patterned illumination allows for a relatively small number of sources while providing high-spatial sampling for high quality reconstruction[10]. As expected, the total computation time for the pMC method (with 10^9 photons, 7.3 h) is more than the aMC method (with 10^8 photons, 2 h) for this specific gate used in reconstruction. However, if more gates are selected in reconstruction, the pMC method can be faster due to the convolution time in the aMC method. Moreover, the N_s/N_d ratio is 1.52 in this reconstruction, while all of the pixels from the CCD (up to 1340×1020) can be applied in reconstructions resulting in shorter calculation times for the pMC method compared to the aMC method. Note that in the CW case, the computational time for the pMC method is 43 minutes and 12 min for the pMC and aMC methods, respectively.

IV. CONCLUSION

In this work, we first demonstrate that the pMC and aMC approaches can be employed for tomographic reconstruction in a acceptable computational time frame, where as the mMC method is computationally unpractical. Second, the effect of different parameters on the statistics of the Jacobians calculated by the aMC and pMC methods are evaluated. The influence of the number of photons on statistics is different for the aMC and pMC methods. Increasing the μ_s' will decrease the statistical stability. In time-domain, the statistics does not change significantly as gate position varies for the pMC method while the aMC method shows a better performance for late gates. Third, the pMC method is found to be more efficient when a large number of detectors or full time-gated dataset are employed, such as the data set acquired by a CCD camera, while the aMC method is best suited for smaller number of SD pairs ($<50 \times 200$) and less number of gates. While wide-field tomography is emerging in FMT with a smaller dataset containing comprehensive information is acquired,[22,24] the adjoint method might be employed in reconstructions more intensively. Moreover, with the recent progress of Monte Carlo simulation using GPU (Refs. 25 and 26) (only for the aMC method), it is expected that a full reconstruction can be finished on a typical personal computer in the time frame comparable to the classic diffusion equation based models ($\sim$ 1 h).

ACKNOWLEDGMENTS

This work has been funded by NCI grant R21 CA161782. The authors gratefully acknowledge the support of the Computational Center for Nanotechnology Innovations at Rensselaer Polytechnic Institute (RPI).

[a]Electronic mail: intesx@rpi.edu

[1]K. M. Yoo, F. Liu, and R. R. Alfano, "When does the diffusion approximation fail to describe photon transport in random media?," Phys. Rev. Lett. **65**, 2210–2211 (1990).
[2]T. Pan, J. C. Rasmussen, J. H. Lee, and E. M. Sevick-Muraca, "Monte carlo simulation of time-dependent, transport-limited fluorescent boundary measurements in frequency domain," Med. Phys. **34**, 1298–1311 (2007).
[3]C. K. Hayakawa and J. Spanier, "Perturbation Monte Carlo methods to solve inverse photon migration problems in heterogeneous tissues," Opt. Lett. **26**, 1335–1337 (2001).
[4]J. Chen and X. Intes, "Time-gated perturbation Monte Carlo method for whole body imaging in small animals," Opt. Express **17**, 19566–19579 (2009).
[5]A. T. N. Kumar, S. B. Raymond, A. K. Dunn, B. J. Bacskai, and A. B. Boas, "A time domain fluorescence tomography system for small animal imaging," IEEE Trans. Med. Imaging **27**, 1152–1163 (2008).
[6]S. B. Raymond, D. A. Boas, B. J. Basckai, and Anand T. N. Kumar, "Lifetime-based tomographic multiplexing," J. Biomed. Opt. **15**, 046011 (2010).
[7]J. Chen, V. Venugopal, and X. Intes, "Monte Carlo based method for fluorescence tomographic imaging with lifetime multiplexing using time gates," Biomed. Opt. Express **2**, 871–886 (2011).
[8]X. Zhang, C. T. Badea, and G. A. Johnson, "Three-dimensional reconstruction in freespace whole-body fluorescence tomography of mice using optically reconstructed surface and atlas anatomy," J. Biomed. Opt. **14**, 064010 (2009).
[9]M. Niedre and V. Ntziachristos, "Comparison of fluorescence tomographic imaging in mice with early-arriving and quasi-continuous-wave photons," Opt. Lett. **35**, 369–371 (2010).
[10]V. Venugopal, J. Chen, F. Lesage, and X. Intes, "Full-field time-resolved fluorescence tomography of small animals," Opt. Lett. **35**, 3189–3191 (2010).

[11]K. Suhling, P. French, and D. Phillips, "Time-resolved fluorescence microscopy," Photochem. Photobiol. Sci. **4**, 13–22 (2005).
[12]S. R. Arridge, "Optical tomography in medical imaging," Inverse Probl. Eng. **15**, 41–63 (1999).
[13]C. K. Hayakawa, J. Spanier, and V. Venugopalan, "Coupled forward-adjoint monte carlo simulations of radiative transport for the study of optical probe design in heterogeneous tissues," J. Appl. Math. **68**, 253–270 (2007).
[14]A. T. N. Kumar, S. B. Raymond, G. Boverman, D. A. Boas, and B. J. Bacskai, "Time resolved fluorescence tomography of turbid media based on lifetime contrast," Opt. Express **14**, 12255–12270 (2006).
[15]R. J. Crilly, W. F. Cheong, B. Wilson, and J. R. Spears, "Forward-adjoint fluorescence model: Monte carlo integration and experimental validation," Appl. Opt. **36**, 6513–6519 (1997).
[16]I. Serov, T. John, and J. Hoogenboom, "A midway forward-adjoint coupling method for neutron and photon monte carlo transport," Nucl. Sci. Eng. **133**, 55–72 (1999).
[17]I. Serov, T. John, and J. Hoogenboom, "A new effective Monte Carlo midway coupling method in mcnp applied to a well logging problem," Appl. Radiat. Isot. **49**, 1737–1744 (1998).
[18]A. J. Welch, C. M. Gardner, R. Richards-Kortum, E. Chan, G. Criswell, J. Pfefer, and S. Warren, "Propagation of fluorescent light," Lasers Surg. Med. **21**, 166–178 (1997).
[19]E. Alerstam, S. Andersson-Engels, and T. Svensson, "White Monte Carlo for time-resolved photon migration," J. Biomed. Opt. **13**, 041304 (2008).
[20]G. Alexandrakis, F. R. Rannou, and A. F. Chatsiioannou, "Tomographic bioluminescence imaging by use of a combined optical-pet (opet) system: a computer simulation feasibility study," Phys. Med. Biol. **50**, 4225–4241 (2005).
[21]V. Venugopal, J. Chen, and X. Intes, "Development of an optical imaging platform for functional imaging of small animals using wide-field excitation," Biomed. Opt. Express **1**, 143 (2010).
[22]J. Chen, V. Venugopal, F. Lesage, and X. Intes, "Time-resolved diffuse optical tomography with patterned light illumination and detection," Opt. Lett. **35**, 125112 (2010).
[23]M. Hopf and T. Ertl, "Accelerating 3D convolution using graphics hardware," *Proceedings of the 10th IEEE Visualization Conference*, (IEEE Computer Society Press, Los Alamitos, CA, 1999).
[24]S. Belanger, M. Abran, X. Intes, C. Casanova, and F. Lesage, "Realtime diffuse optical tomography based on structured illumination," J. Biomed. Opt. **15**, 016006 (2010).
[25]E. Alerstam, T. Svensson, and S. Andersson-Engels, "Parallel computing with graphics processing units for high-speed Monte Carlo simulation of photon migration," J. Biomed. Opt. **13**, 060504 (2008).
[26]Q. Fang and A. B. Boas, "Monte Carlo simulation of photon migration in 3D turbid media accelerated by graphics processing units," Opt. Express **17**, 20178–20190 (2009).